In Vivo Cancer Dual-Targeting and Dual-Modality Imaging with Functionalized Quantum Dots

Kongzhen Hu*[1], Hongliang Wang*[1], Ganghua Tang[1], Tingting Huang[1], Xiaolan Tang[2], Xiang Liang[1], Shaobo Yao[1], and Dahong Nie[1]

[1]*PET-CT Center, Department of Nuclear Medicine, the First Affiliated Hospital, Sun Yat-Sen University, Guangzhou, China; and* [2]*College of Science, Southern China Agricultural University, Guangzhou, China*

Semiconductor quantum dots (QDs), after surface modification to provide water solubility and biocompatibility, have a promising future in biomedical applications. In this study, a dual receptor–targeting dual-modality PET/near-infrared fluorescence (NIRF) probe was developed for accurate assessment of the pharmacokinetics and tumor-targeting efficacy of QDs. **Methods:** QDs were modified by β-Glu-RGD-BBN (RGD is arginine-glycine-aspartate acid, and BBN is bombesin) peptides and then labeled with ^{18}F via the 4-nitrophenyl-2-^{18}F-fluoropropionate prosthetic group. Cytotoxicity and cell-binding assay of QD-RGD-BBN were performed with PC-3 cells. In vivo dual-modality PET/NIRF imaging of prostate tumor–bearing mice was investigated using QD-RGD-BBN and 2-^{18}F-fluoropropionyl-QD-RGD-BBN (^{18}F-FP-QD-RGD-BBN). An in vivo biodistribution study of ^{18}F-FP-QD-RGD-BBN was performed on normal mice. **Results:** QD-RGD-BBN exhibited strong red luminescence (600–800 nm) with the same maximum fluorescence wavelength (705 nm) as QD705 and slightly lower toxicity than that of QD705 in PC-3 cells at concentrations of greater than 30 μg/mL. Uptake of QD-RGD-BBN in PC-3 cells showed no significant decrease in the presence of an excess amount of dimer arginine-glycine-aspartate acid (RGD_2) or bombesin(7–14) (BBN) peptide but was blocked significantly in the presence of an excess amount of NH_2-RGD-BBN. Dual-function PET/NIRF imaging is able to accurately assess the biodistribution and tumor-targeting efficacy of the ^{18}F-labeled functionalized QDs. **Conclusion:** The functionalized QD probe has great potential as a universal dual-targeting probe for detecting tumors in living subjects, opening up a new strategy for the development of multitargeting multimodality ^{18}F-labeled QD probes with improved tumor-targeting efficacy.

Key Words: quantum dots; fluorescence; PET; integrin $\alpha_v\beta_3$; GRPR

J Nucl Med 2015; 56:1278–1284
DOI: 10.2967/jnumed.115.158873

Quantum dots (QDs) are photoluminescent semiconductor nanocrystals and have extraordinary fluorescent properties including high brightness, high resistance to photobleaching, tunable wavelengths, and high levels of photostability (*1*). The recently developed cadmium telluride QDs, with fluorescence emission in the near-infrared range (600–800 nm), are ideal for in vivo imaging to avoid tissue autofluorescence. In vivo specific tumor targeting has been achieved with various QD-based conjugates linked with biorecognition ligands such as peptides, antibodies, nucleic acids, or small-molecule inhibitors for application as fluorescent probes (*2–6*). QD probes conjugated with tens or even hundreds of ligands on the surface of 1 QD may exhibit strong binding affinity and good targeting efficacy because of the polyvalency effect. Given the multiple raised biomarkers (targets) of tumor cells, development of a probe simultaneously targeting 2 or more biomarkers will be a new strategy for the imaging application (Fig. 1) (*7*). Generally, there are 2 possible approaches to endow the new profile of the QD probe. One approach is to conjugate QDs with multiple ligands for targeting multiple biomarkers (or receptors) on the tumor cells and chelating agents by QD multiplex modifications before the QD conjugate is labeled with the imaging signal groups (such as radionuclide, fluorophore) (Fig. 1A, left). For example, the QDs with an amine-functionalized surface are conjugated with both arginine-glycine-aspartate acid (RGD) peptide for targeting integrin $\alpha_v\beta_3$ and chelating agent DOTA for binding ^{64}Cu, respectively (*8*). Another approach is to conjugate QDs with a prefabricated heteropolymer from multiple ligands for tumor-targeting biomarkers and chelators for binding imaging signal groups by a single modifying QD procedure before the QD conjugate is labeled with the imaging signal groups (Fig. 1A, middle).

Integrin $\alpha_v\beta_3$ is overexpressed in a variety of solid tumor types, such as melanoma; late-stage glioblastoma; and breast, prostate, lung, and ovarian cancers (*9*) but is not readily detectable in resting endothelial cells or most normal organs, which makes it a universally applicable target for molecular imaging and therapy of cancer. Synthetic peptides containing the RGD sequence motif are active modulators of cell adhesion and can bind specifically to integrin $\alpha_v\beta_3$ (*10*). Gastrin-releasing peptide receptor (GRPR) primarily overexpressed in androgen-independent human prostate tissues (*11*) provides another potential target for prostate cancer diagnosis and therapy. Bombesin is an analog of gastrin-releasing peptide and the truncated sequence bombesin(7–14) (BBN) is considered to be capable of the specific binding to GRPR and metabolically stable for in vivo application (*12,13*). During the processes of angiogenesis, invasion, and metastasis of the GRPR-positive tumors, the activated endothelial cells around the tumor tissues can express a high level of integrin $\alpha_v\beta_3$. Therefore, the GRPR-positive tumors are dual integrin and GRPR receptor–positive. Several radiolabeled hybrid RGD and BBN peptides have been

Received Apr. 6, 2015; revision accepted Jun. 17, 2015.
For correspondence or reprints contact either of the following:
Ganghua Tang, Department of Nuclear Medicine, the First Affiliated Hospital, Sun Yat-Sen University, Guangzhou, 510080, China.
E-mail: gtang0224@126.com
Dahong Nie, Department of Nuclear Medicine, the First Affiliated Hospital, Sun Yat-Sen University, Guangzhou, 510080, China.
E-mail: niedahong@126.com
*Contributed equally to this work.
Published online Jun. 25, 2015.

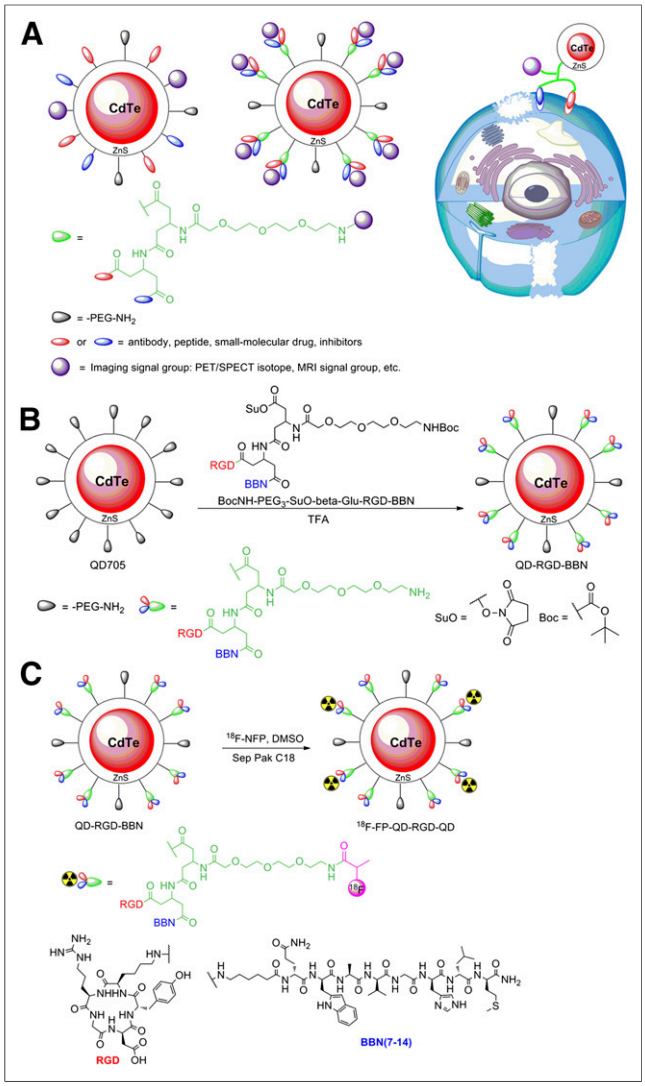

FIGURE 1. (A) Schematic illustration of functionalized QD probe for in vivo cancer dual-targeting and dual-modality imaging: structure of multiplex modifying multifunctional QD probe (left), structure of single modifying multifunctional QD probe (middle), and strategy for enhancing synergistic binding of heterodimeric multifunctional QD probe (right). (B) Synthesis of QD-RGD-BBN. (C) Synthesis of dual receptor–targeting dual-modality PET probe ^{18}F-FP-QD-RGD-BBN. CdTe = cadmium telluride; DMSO = dimethyl sulfoxide; TFA = trifluoroacetic acid.

developed for functional imaging of integrin $\alpha_v\beta_3$ and GRPR expression (*14,15*). However, the dual-targeting QD probe for dual-modality imaging of integrin $\alpha_v\beta_3$ and GRPR has not been reported thus far.

We have reported multitargeting multifunction molecular imaging of bioconjugated nanoprobes with a symmetric β-glutamate (β-Glu) group and a tripolyethylene glycol (PEG_3) spacer prepared by the single modifying approach (*16,17*). In this study, we developed bioconjugated QD probes suitable for in vivo dual-targeting and dual-modality imaging of cancer cells growing in mice. This new class of functionalized QD probes prepared by the single modifying approach contains dual integrin $\alpha_v\beta_3$– and GRPR-targeting ligands for tumor receptor recognition as well as symmetric β-Glu groups and multiple polyethylene glycol molecules for improving biocompatibility, circulation, and labeling. We examined the biodistribution, nonspecific uptake, cellular toxicity, and pharmacokinetics of these highly stable and bright QD probes in cells and animal models. Moreover, the in vivo dual-modality PET/near-infrared fluorescence (NIRF) imaging of prostate tumor–bearing mice was investigated using a Glu-RGD-BBN–modifying QD probe (QD-RGD-BBN) and ^{18}F-labeled RGD-BBN hybrid-peptide–modifying QD probe 2-^{18}F-fluoropropionyl-QD-RGD-BBN (^{18}F-FP-QD-RGD-BBN). The dual-targeting dual-function molecular imaging allows for the accurate assessment of the biodistribution and tumor-targeting efficacy of the functionalized QDs. The functionalized QD probe opens new possibilities for the development of multitarget multifunction probes with improved tumor-targeting efficacy.

MATERIALS AND METHODS

Materials

Amine-modified QD705 was purchased from Quantum Dot Corp. (emission maximum at 705 nm). The Inveon small-animal PET/CT scanner was purchased from Siemens. A laser scanning confocal microscope (LSM710) was purchased from Zeiss. The Caliper Life Sciences IVIS imaging system was purchased from Caliper Life Sciences Inc. The Microplate reader was purchased from Tecan Sunrise.

Animals

Female athymic BALB/c (strain *nu/nu*) nude mice (n = 18; age, 6–8 wk; weight, 20–25 g) and Kunming mice (body weight range, 18–25 g) were purchased from the Experimental Animal Center of Sun Yat-Sen University (China). The mice were bred in constant temperature and humidity conditions. Feeds, beds, and drinking water were sterilized. All animal experimental studies were approved by the Institutional Animal Care and Use Committee of the First Affiliated Hospital, Sun Yat-Sen University (approval no. [2012]001 and no. [2013]A-173). All efforts were made to minimize animal suffering, to reduce the number of animals used, and to use alternatives to in vivo techniques, if available.

Preparation of ^{18}F-FP-QD-RGD-BBN

QD-RGD-BBN was synthesized stepwise by a solid-phase peptide synthesis method described in the supplemental information (available at http://jnm.snmjournals.org) (*16,17*). 4-nitrophenyl-2-^{18}F-fluoropropionate (^{18}F-NFP) was prepared according to the previously reported procedure (*18,19*). Radiosynthesis of ^{18}F-FP-QD-RGD-BBN followed the modified reported procedure in the supplemental information (*19*).

Cytotoxicity

The cytotoxicity of QD705 and QD-RGD-BBN was examined in PC-3 cells using the Cell Counting Kit-8 (KeyGen Biotech) according to the instruction of the manufacturer. Cells were seeded at a density of 1.0×10^4 cells/well in 96-well plates, allowed to grow for 24 h, and exposed to various concentrations of QD705 and QD-RGD-BBN for 24 h. The absorbance of each well at 450 nm was measured with an absorbance microplate reader.

In Vitro Binding Studies

The in vitro cell fluorescence staining was performed following the previously reported procedure (*2*). Cold 4% phosphate-buffered paraformaldehyde-fixed PC-3 cells were stained with 1 nM QD705 and 1 nM QD-RGD-BBN or with 1 nM QD-RGD-BBN in the presence of 2 μM dimer peptide RGD_2, BBN, and heterodimer NH_2-RGD-BBN (or the mixture of 2 μM BBN and 2 μM RGD_2). The cells were then examined under the confocal laser scanning microscope (excitation, 420 nm; emission, 705 nm).

In Vivo NIRF Imaging

Athymic nude mice bearing PC-3 prostate cancer were anesthetized with 5% chloral hydrate solution (6 mL/kg) and injected with QD-RGD-BBN in 100 μL of saline via the tail vein. In vivo optical imaging was performed with the Caliper Life Sciences IVIS Imaging System. Images were acquired at different time points after injection. Each acquisition took 5 min for all studies. Images were analyzed using Living Image 3.0 software (Caliper Life Sciences). The optical signal was normalized to p/s/cm^2/sr.

In Vivo Biodistribution

The method of in vivo biodistribution was similar to that reported previously (*18*). Detailed procedures for studying in vivo biodistribution of ^{18}F-FP-QD-RGD-BBN using Kunming mice are included in the supplemental information.

In Vivo PET Imaging

PET/CT imaging studies with tumor-bearing mice were performed using the Inveon small-animal PET/CT scanner. The mice were anesthetized with a 5% chloral hydrate solution (6 mL/kg). ^{18}F-FP-QD-RGD-BBN (3.7−7.4 MBq) was injected intravenously via the tail. The animals were placed on a heating pad to maintain body temperature throughout the procedure and visually monitored for breathing and any other signs of distress throughout the entire imaging period. Ten-minute static PET images were acquired at 4 time points (30, 60, 90, and 120 min) after injection. Imaging started with a low-dose CT scan, immediately followed by a PET scan. The CT scan was used for attenuation correction and localization of the lesion site. The images were reconstructed by 2-dimensional ordered-subsets expectation maximum. For each small-animal PET scan, regions of interest (ROIs) were drawn over the tumor and major organs on decay-corrected whole-body coronal images using Inveon Research Workplace 4.1 (Siemens) software. The radioactivity concentration (accumulation) within a tumor or an organ was obtained from mean pixel values within the multiple-ROI volume, which were converted to MBq/mL using a conversion factor. Assuming a tissue density of 1 g/mL, the ROIs were converted to MBq/g and then divided by the administered activity to obtain an imaging ROI-derived percentage injected dose per gram of tissue (%ID/g).

Statistical Analysis

Data were expressed as mean ± SEM, and the significance of comparison between 2 datasets was determined using the Student *t* test (Prism, version 5.0; GraphPad Software) and defined as significant ($0.01 < P < 0.05$), very significant ($0.001 < P < 0.01$), and extremely significant ($P < 0.001$).

RESULTS

Modification and Radiolabeling of QDs

QD-RGD-BBN was prepared from the coupling reaction of QD705 with peptide heterodimer BocNH-PEG$_3$-SuO-β-Glu-RGD-BBN (Fig. 1B; Supplemental Fig. 1). Briefly, the modified QD705 was reacted with the activated ester group (BocNH-PEG$_3$-SuO-β-Glu-RGD-BBN) in a borate buffer solution (2 mM, pH 8.5) and then added to trifluoroacetic acid (3 mL) at 0°C and stirred for 2 h. After the removal of excess trifluoroacetic acid under reduced pressure, the final product QD-RGD-BBN was purified using size-exclusion chromatography. Both QD705 and QD-RGD-BBN were resuspended in phosphate-buffered saline solution (pH 7.4) to form a stock solution of 1 mg/mL for further investigation.

QD-RGD-BBN was radiolabeled using ^{18}F-NFP as the prosthetic group, to get ^{18}F-FP-QD-RGD-BBN (Fig. 1C). The decay-corrected radiochemical yield was 40% from ^{18}F-NFP, and the radiochemical purity was more than 95%. Coinjection of ^{18}F-FP-QD-RGD-BBN and nonradioactive FP-QD-RGD-BBN assessed the identity of the radiopharmaceutical with an ultraviolet ray detection of 254 nm. The chemical synthesis of the standard was based on the above procedure, which was purified by semi-preparative high-performance liquid chromatography and confirmed using mass spectroscopy. Furthermore, in vitro stability experiments showed that ^{18}F-FP-QD-RGD-BBN in saline and mice serum at 37°C for 2 h was more than 95% of radiochemical purity by radio–high-performance liquid chromatography analysis, similar to ^{18}F-FP-QD-705 (*16*).

Characterization and Cytotoxicity of QD-RGD-BBN

On the basis of dynamic light scattering measurements, the average diameter of QD705 was 32.8 nm and average diameter of QD-RGD-BBN was 123.5 nm (Fig. 2). It has been reported that the measured particle diameter sizes of cadmium selenide and QD nanocrystals using atomic force microscopy are significantly smaller than those determined by transmission electron microscopy (*2,20*). In this study, we observed that the measured diameter sizes of QD705 and QD-RGD-BBN using dynamic light scattering were smaller than those determined by transmission electron microscopy. QD-RGD-BBN exhibited exceptionally strong red luminescence (600–800 nm, Fig. 2C) with the same maximum fluorescence wavelength (705 nm) as QD705, which is suitable for in vivo optical imaging with deep-tissue penetration. The ultraviolet visible absorbance spectra of NH_2-RGD-BBN, QD705, and QD-RGD-BBN in phosphate-buffered saline solution are shown in Figure 2D. Given the maximum absorption of the peptide NH_2-RGD-BBN at 220 nm, the QD-RGD-BBN absorption peaks appearing at 220 nm demonstrated the successful conjugation with NH_2-RGD-BBN in the surface of QD705.

The cytotoxicity of QDs was always an important consideration before its application to cellular or in vivo study. Within the QD probe concentration of 50 μg/mL, the toxicity of QD705 and QD-RGD-BBN was low and amenable for cellular imaging (Supplemental Fig. 2). The toxicity of QD705 was slightly higher than that of

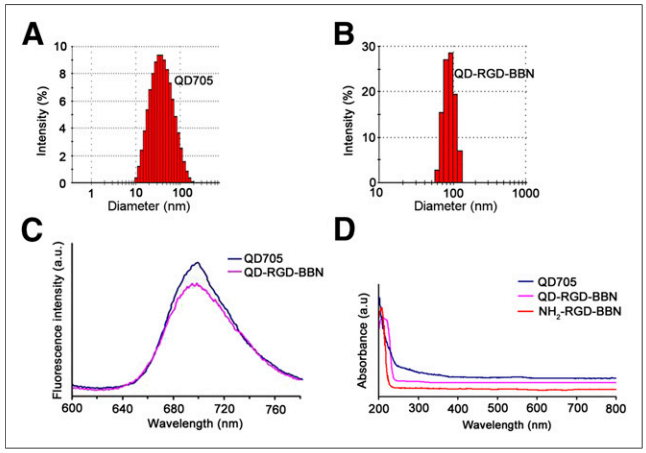

FIGURE 2. Characterization of QD probes. (A) Dynamic light scattering data of QD705. (B) Dynamic light scattering data of QD-RGD-BBN. (C) Fluorescence spectra of QD-RGD-BBN and QD705 in aqueous solution. (D) Ultraviolet visible absorbance spectra of NH_2-RGD-BBN, QD-RGD-BBN, and QD705.

QD-RGD-BBN in PC-3 cells at concentrations of greater than 30 μg/mL. Higher exposure to zinc sulfide may have been the reason for the enhanced toxicity of QD705 in PC-3 cells.

In Vitro Cell Staining

To investigate the cancer cell–targeting characteristics of the multifunctionalized fluorescence probe QD-RGD-BBN, we took advantage of its fluorescence. PC-3 human prostate cancer cells (both integrin $\alpha_v\beta_3$ and GRPR co-overexpression) were used. As shown in Figure 3, intense fluorescence signals on PC-3 cells were observed for QD-RGD-BBN but not for the unconjugated QD705. Blocking with the RGD_2 or BBN peptide resulted in no significant decrease of fluorescence signal in cells, whereas blocking with NH_2-RGD-BBN (or the mixture of BBN and RGD_2) showed significantly decreased fluorescence signal on staining cells. This finding confirmed the high binding affinity and specificity of QD-RGD-BBN to dual-receptor integrin $\alpha_v\beta_3$ and GRPR in prostate cancer.

In Vivo NIRF Imaging

Such promising in vitro findings warrant further investigation of QD-RGD-BBN probes for in vivo imaging applications, where they may serve as nanoplatforms for image-guided tumor vasculature and GRPR-targeted drug delivery. For in vivo optical imaging, fluorescence emission of QD-RGD-BBN (maximum, 705 nm) is in the near-infrared (700–900 nm) region. The optical imaging of the animal models with the QD conjugate probe is seen in Figure 4. There was steady increased fluorescence intensity in the tumors of mice injected with QD-RGD-BBN (Fig. 4A) within several hours after injection. At 30 min after injection, a slight fluorescence signal of QD-RGD-BBN was observed in the tumor. At 5 h after injection, the tumor signal intensity reached its maximum. The ratio of tumor to background (muscle) was 2.08 ± 0.12 (Fig. 4B, the background referred to the hind limb muscle, $n = 3$). However, no significant fluorescence signals of QD705 were observed in the tumor, and the significant clearance was found after 5 h after injection (Supplemental Fig. 3). The tumor-to-background ratio of QD705 was 0.80 ± 0.07 at 5 h after injection ($n = 3$) (Fig. 4B). In addition, the tissue uptake rate of QD-RGD-BBN was slow because of long blood distributed circulation, leading to a slow increased accumulation of the QD conjugate probe in the tumors within 5 h after injection (*2,8*). Therefore, the tumor NIRF imaging demonstrated successful in vivo tumor targeting use of QD-RGD-BBN.

Ex Vivo NIRF Imaging

To study the distribution and targeting characteristics of QD-RGD-BBN, ex vivo NIRF imaging was performed. The best tumor contrast was observed at 5 h after injection of QD-RGD-BBN and the model mice were sacrificed and most major tissues were harvested and imaged immediately at 5 h after injection of QD705 and QD-RGD-BBN. The IVIS Imaging System was used for ex vivo NIRF imaging (excitation, 420 nm; emission, 705 nm). The fluorescence signal intensity for ex vivo imaging truly reflected the retained QD probes (without the autofluorescence) in model mice. As can be seen in Figure 5A, the fluorescence signals were clearly visible in the PC-3 tumor, liver, lung, and kidney of the mice injected with QD-RGD-BBN. Low signal intensity for stomach and skin were observed (stomach could be caused by the food and skin could be caused by autofluorescence) (Fig. 5A). On the contrary, no fluorescence signal was seen in tumors of the mice injected with QD705, but high signals in the liver, spleen, and bone were observed (Fig. 5B).

To further understand the distribution pattern and binding characteristics of QD probes in vivo and compare the fluorescence intensity between different tissues, tumor tissue, brain, bone, heart, spleen, liver, kidney, and muscle were frozen in optimal-cutting-temperature medium and cryosectioned at −20°C into sections (8 μm thick) using a cryosection system (Shandon Cryotome FSE; Thermo Fisher Scientific), fixed with acetone at 0°C, and examined with the confocal laser scanning microscope. Comparative histologic data of tissues of mice injected with QD probes are shown in Supplemental Figure 4. As shown from the red fluorescence of QD probes, nonspecific QD705 uptake and retention took place primarily in the liver, bone, and spleen, without significant accumulations in the brain, heart, kidney, or muscle, indicating high accumulations in the major organs of the reticuloendothelial system. This pattern of in vivo tissue uptake and distribution of QD705 was similar to that of other reported QD nanoparticles (*21,22*) in coincidence with the ex vivo NIRF imaging result above. In comparison to QD-RGD-BBN, there was no significant fluorescence in tumors for QD705. For QD-RGD-BBN, the QD-conjugated probe was delivered and significantly retained by the tumor tissue and nonspecific liver. Nonspecifically low uptake in the spleen and bone was also observed, which was consistent

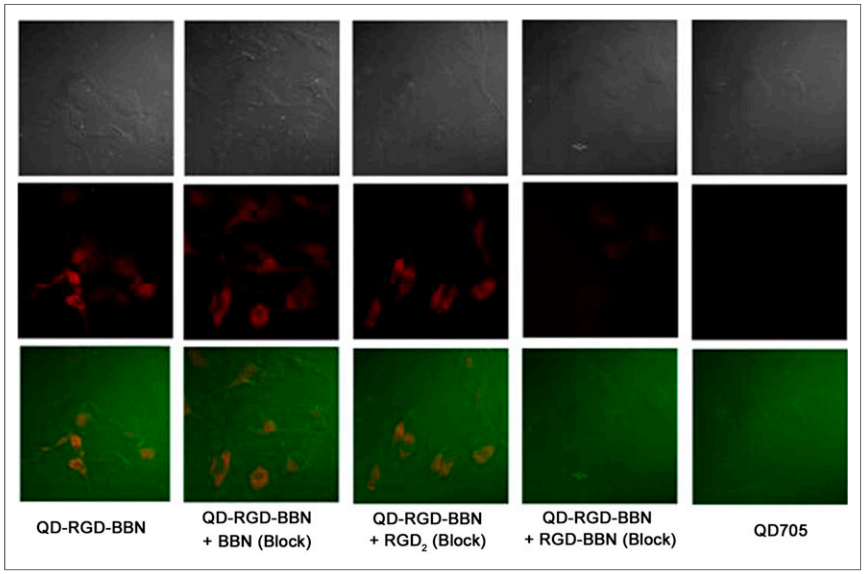

FIGURE 3. In vitro staining of PC-3 cells (both integrin $\alpha_v\beta_3$ and GRPR high expression) using 1 nM QD-RGD-BBN (left-first column) and 1 nM QD705 (right-first column). Staining of PC-3 cells with 1 nM QD-RGD-BBN in presence of 2 μM BBN (QD-RGD-BBN + BBN Block), 2 μM RGD_2 (QD-RGD-BBN + RGD_2 Block), and mixture of 2 μM BBN and 2 μM RGD_2 (QD-RGD-BBN + RGD-BBN Block) is also shown. Filter set: excitation, 420/40 nm; emission, 705/40 nm. Magnification, ×400, 0.5-s exposure. All fluorescence images were acquired under same condition and displayed under same scale.

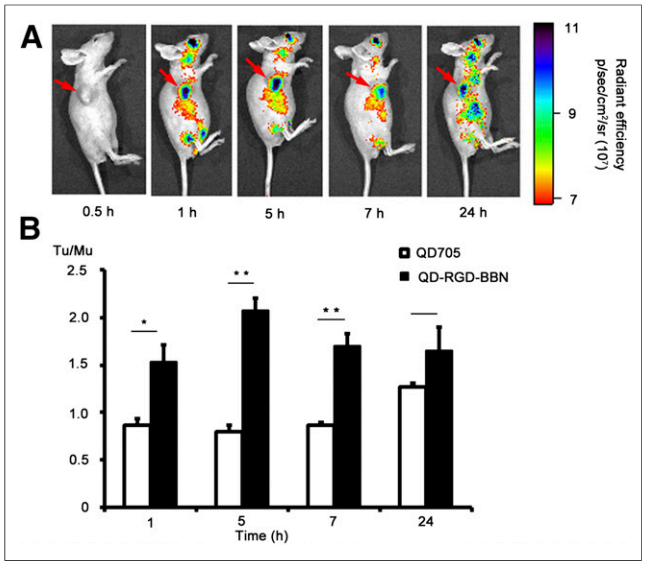

FIGURE 4. (A) In vivo NIRF imaging of PC-3 tumor–bearing mice at 0.5, 1, 5, 7, and 24 h after injection of 200 pmol QD-RGD-BBN. Arrows indicate tumor. (B) Tumor-to-muscle uptake ratios (Tu/Mu) of mice injected with QD705 and QD-RGD-BBN. Data are mean ± SD. $^{*}P < 0.05$, as compared with mice injected with QD705, 1-tailed paired Student t test ($n = 3$). $^{**}P < 0.01$.

with the above ex vivo NIRF imaging result. The heterogeneous red fluorescence of QDs could be attributed to the diameter of the QDs without enough extravasation into cells from the tumor vasculature (*21*).

In Vivo Biodistribution

Attaching PET isotopes to QD conjugates is highly beneficial because PET is sensitive, quantitative, and clinically relevant with ultrahigh tissue penetration. The in vivo biodistribution of ^{18}F-FP-QD-RGD-BBN is shown in Table 1. At 5 min after injection, ^{18}F-FP-QD-RGD-BBN was rapidly absorbed almost in all the tissues, with high uptake in the kidneys and liver. From 5 to 120 min after injection, radioactivity accumulation in the kidneys and liver decreased significantly, indicating that the tracer was excreted mainly through the renal and liver pathway. ^{18}F-FP-QD-RGD-BBN showed a moderate lung, blood, and intestine uptake with a relatively slow washout rate. In addition, low radioactivity accumulations in the brain, spleen, pancreas, and bone were found after 30 min after injection.

In Vivo PET Imaging

The representative transaxial and coronal PET images are shown in Figure 6A. The tumor was clearly delimitated, with significant radioactivity accumulation after 30 min after injection of ^{18}F-FP-QD-RGD-BBN (Figs. 6A and 6B). PET imaging provided the consistent distribution data obtained from the in vivo biodistribution result of ^{18}F-FP-QD-RGD-BBN. Radioactivity accumulation of tumor, brain, and muscle in PC-3 tumor–bearing mice was measured from ROIs encompassing the entire organ on the small-animal PET coronal images. The tumor had the highest radioactivity accumulation at 60 min after injection. However, the radioactivity accumulation in brain and muscle decreased from 30 to 120 min after injection (Figs. 6A and 6B). Tumor uptake of ^{18}F-FP-QD-RGD-BBN at 60 min after injection was significantly decreased in the presence of RGD-BBN (control group), compared with the absence of blocking agent (Fig. 6C). ^{18}F-FP-QD-RGD-BBN also showed tumor-targeting efficiency similar to QD-RGD-BBN, with high accumulation in PC-3 tumor tissue.

DISCUSSION

Multiple-modality imaging provides a new prospective for in vivo imaging. Various modified QD probes are feasible for optical imaging and can also be conjugated with a variety of reporter signals for other imaging modalities including nuclear (*8*) and MR imaging (*23–25*). Meanwhile, molecular imaging of multiple targets will be another effective approach to improve the efficacy of targeting imaging. We have prepared a novel nontoxic symmetric β-Glu linker for the synthesis of peptide dimer β-Glu-RGD$_2$ (*19*) and peptide heterodimer BBN-β-Glu-RGD, due to β-Glu as a substrate for glutamine synthetase (*26*). To further enhance the ^{18}F-labeling yield and to improve the in vivo kinetics, a tripolyethylene glycol spacer was attached to the glutamate β-amino group of β-Glu-RGD-BBN, and ^{18}F-FP-QD-RGD-BBN was prepared by the reaction of QD-RGD-BBN with ^{18}F-NFP in this study.

In this study, we reported on synergistic targeting integrin $\alpha_v\beta_3$ and GRPR of dual-function QD probe QD-RGD-BBN for in vitro cell staining. The PC-3 cell staining with QD-RGD-BBN was slightly inhibited in the presence of an excess amount of unlabeled BBN and RGD$_2$, respectively, which contributed to the high coexpression of both integrin $\alpha_v\beta_3$ and GRPR in PC-3 cells. However, the PC-3 cells stained with QD-RGD-BBN were blocked completely in the presence of the mixture of BBN and RGD$_2$ (or RGD-BBN), showing that QD-RGD-BBN could specifically target both integrin $\alpha_v\beta_3$ and GRPR. In the blocking experiment, the result further confirmed radiolabeled QD-RGD-BBN dual-targeting to both integrin $\alpha_v\beta_3$ and GRPR (Fig. 6). For the in vivo and ex vivo NIRF imaging, there were certainly different delivery kinetics of the tumor and tissues between QD705 and QD-RGD-BBN. QD705 had almost no uptake in the tumor,

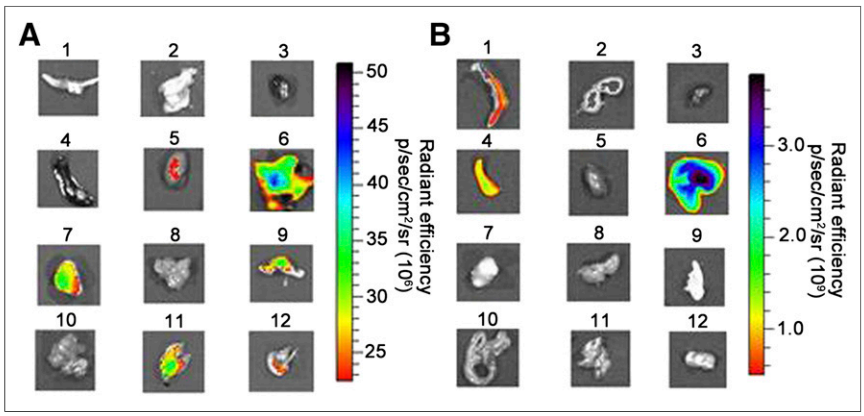

FIGURE 5. Ex vivo NIRF imaging. (A) NIRF image of harvested major organs at 5 h after injection of QD-RGD-BBN. (B) NIRF image of harvested major organs at 5 h after injection of QD705. 1 = bone; 2 = brain; 3 = heart; 4 =spleen; 5 = kidney; 6 = liver; 7 = tumor; 8 = muscle; 9 = skin; 10 = intestine; 11 = lung; 12 = stomach.

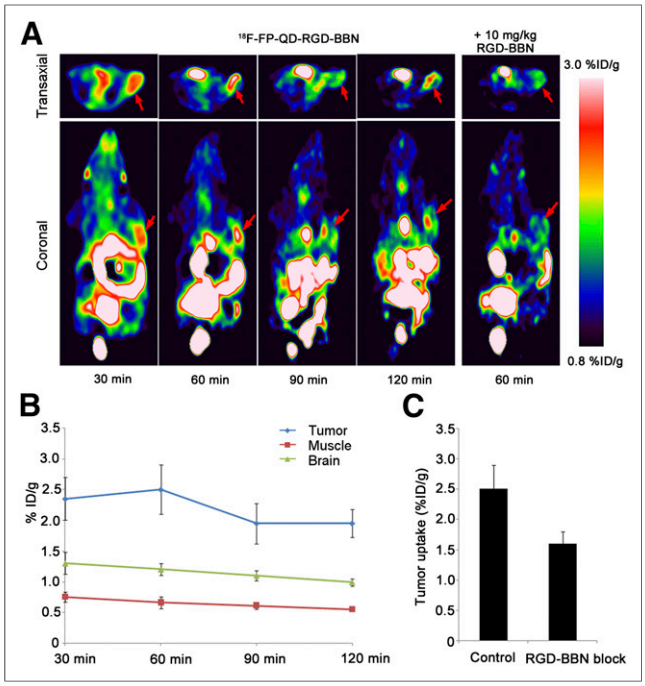

FIGURE 6. PET imaging of PC-3 tumor–bearing mice with targeting dual-receptor PET/NIRF probe. (A) PET images of same mouse at 30, 60, 90, and 120 min after injection of ^{18}F-FP-QD-RGD-BBN and in presence of blocking agent RGD-BBN. Red arrows indicate tumor. (B) Uptake of ^{18}F-FP-QD-RGD-BBN in tumor, muscle, and brain over time, as quantified by ROI analysis of small-animal PET scans (n = 3 per group). (C) Tumor uptake of ^{18}F-FP-QD-RGD-BBN at 60 min after injection in absence of blocking agent (control) and in presence of RGD-BBN, as quantified by ROI analysis of small-animal PET scans (n = 3 per group). %ID/g = percentage injected dose per gram.

kidney, and lung but showed high accumulation in the liver, bone, and spleen of the reticuloendothelial system. However, QD-RGD-BBN showed a slowly increased uptake process of the tumor after 30 min after injection and a slow delivery from blood to liver and lung.

When NIRF imaging was compared with PET imaging in PC-3 tumor–bearing mice, a high accumulation of ^{18}F-FP-QD-RGD-BBN in some tissues such as the kidney, urinary bladder, and liver was observed throughout the PET study. The accumulation discrepancy between PET and optical imaging may be caused by the shedding of the polymer coating from the QD and the metabolic stability of ^{18}F-labeled QD conjugate probe. This accumulation is because the PET scanner measures ^{18}F, but NIRF imaging detects QD fluorescence. The hydrophilic polymer (containing heterodimer peptide and ^{18}F) dual-targeting both integrin $\alpha_v\beta_3$ and GRPR in the PC-3 tumor likely caused the increased tumor uptake, as revealed by NIRF imaging after 1 h after injection and PET imaging after 30 min after injection. Compared with the single receptor–targeting tracer ^{64}Cu-labeled DOTA-QD-RGD, with slow delivery kinetics and no radioactivity uptake in tumors until 5 h after injection (*8*), ^{18}F-FP-QD-RGD-BBN showed rapid kinetic characteristics and clear delineation of the tumor site using PET imaging after 30 min after injection and NIRF imaging after 1 h after injection. It would further support the feasibility of the QD conjugates labeled with short half-time radionuclide ^{18}F. ^{18}F-FP-QD-RGD-BBN offered good pharmacokinetics of low uptake in the abdomen and an excretion pathway different from ^{64}Cu-labeled DOTA-QD-RGD. Moderate radioactivity accumulation in the urinary bladder and high uptake in the liver throughout the PET study indicated that ^{64}Cu-labeled DOTA-QD-RGD was excreted mainly through liver pathways, with minor renal–urinary bladder pathway excretion (*8*). However, a high uptake and fast clearance of ^{18}F-FP-QD-RGD-BBN in the kidneys, liver, and urinary bladder showed that the tracer was excreted mainly through the renal–urinary bladder and liver pathway. Furthermore, ^{18}F-FP-QD-RGD-BBN demonstrated pharmacokinetic characteristics similar to the heterodimer peptide tracer ^{18}F-FB-PEG$_3$-Glu-RGD-BBN (*27*).

The toxicity of QD conjugates is the greatest challenge for in vivo imaging and clinical translation. The major concern is the toxicity of metal elements such as cadmium- and selenium-based QDs conjugates (*8*) and the long-term toxicity in vivo caused by the long half-life of QDs with organic coatings (*23*). It has been reported that the dual-function PET/NIRF probe ^{64}Cu-labeled DOTA-QD-RGD could have a significantly lower potential for toxicity than the NIRF-only QD-based probe (*8*). Additionally, the dual-targeting ^{18}F-labeled PEGylated RGD-bombesin heterodimer ^{18}F-FB-BBN-RGD showed greatly improved tumor-targeting efficacy for signal amplification and favorable pharmacokinetics compared with ^{18}F-labeled RGD and BBN analogs (*14,15,27*). Therefore, the heteropolymer single modifying QD PET imaging approach described in this study requires a much smaller amount of QDs to yield tumor contrast with an advantage of significantly reduced potential cytotoxic risk over NIRF imaging alone, due to the higher sensitivity of PET imaging. In fact, CdTe/zinc sulfide or cadmium selenide/zinc sulfide QD-induced cytotoxicity under the appropriate chemical quantity was not observed in several in vivo and in vitro studies (*28*). No acute and obvious toxicity of QD conjugates was detected in viable cell and animal models in our experiments. It was expected that ^{18}F-FP-QD-RGD-BBN significantly decreased potential cytotoxic risk due to the dual receptor–targeting efficacy for signal amplification, compared with single receptor–based radiolabeled DOTA-QD-RGD.

TABLE 1
In Vivo Biodistribution of ^{18}F-FP-QD-RGD-BBN in Normal Mice

Organ	5 min	30 min	60 min	120 min
Blood	4.57 ± 0.96	3.01 ± 0.50	1.81 ± 0.11	1.73 ± 0.17
Brain	1.89 ± 0.33	1.86 ± 0.20	1.17 ± 0.07	1.04 ± 0.13
Heart	2.51 ± 0.44	1.98 ± 0.12	1.39 ± 0.25	1.36 ± 0.30
Lung	6.87 ± 2.56	3.49 ± 0.74	2.22 ± 0.42	1.50 ± 0.36
Liver	7.03 ± 0.69	3.46 ± 0.84	2.19 ± 0.14	1.98 ± 0.38
Spleen	1.83 ± 0.63	1.62 ± 0.33	1.04 ± 0.20	0.81 ± 0.15
Pancreas	2.73 ± 0.77	1.59 ± 0.43	0.88 ± 0.22	0.61 ± 0.14
Kidneys	10.8 ± 3.82	7.35 ± 1.69	2.60 ± 0.44	1.98 ± 0.34
Intestine	2.56 ± 0.63	3.53 ± 0.69	1.94 ± 0.56	1.56 ± 0.28
Muscle	2.20 ± 0.71	1.51 ± 0.38	0.97 ± 0.09	0.69 ± 0.15
Stomach	2.49 ± 0.68	1.61 ± 0.66	0.96 ± 0.24	0.88 ± 0.10
Bone	1.78 ± 0.61	1.72 ± 0.25	1.04 ± 0.24	0.92 ± 0.14

Data are average percentage injected dose per gram, mean ± SD (n = 4).

CONCLUSION

We have successfully designed and synthesized a dual integrin $\alpha_v\beta_3$– and GRPR-targeting dual-modality PET/NIRF probe, ^{18}F-FP-QD-RGD-BBN, using a heterodimeric peptide single modifying QD procedure. The dual-function PET/NIRF imaging is able to accurately assess the biodistribution and tumor-targeting efficacy of the multifunction QDs. This ^{18}F-labled multifunction QD probe has significantly reduced potential toxicity risk and overcome the tissue-penetration limitation of optical imaging. The strategy for preparation of the functionalized QD probes by the single modifying QD approach may be extended to a general method for preparation and application of other valuable multitargeting QD probes in biomedical and clinical science. The results reported here open up a new avenue for the development of multitarget multifunction probes with improved tumor-targeting efficacy.

DISCLOSURE

The costs of publication of this article were defrayed in part by the payment of page charges. Therefore, and solely to indicate this fact, this article is hereby marked "advertisement" in accordance with 18 USC section 1734. This work was supported by the National Natural Science Foundation of China (no. 81371584, no. 30970856, no. 81471695), Science and Technology Planning Project of Guangzhou (no. 2011J5200025, no. 201510010145), the National High Technology Research and Development Program of China (no. 2008AA02Z430), the Science Technology Foundation of Guangdong Province (no. 2014A020210008, no. 2013B021800264), and the Wu Jieping Medical Foundation (320675013203). No other potential conflict of interest relevant to this article was reported.

ACKNOWLEDGMENTS

We thank Qingqiang Tu, Fuhua Wen, and Kening Wu for their excellent technical support in this work.

REFERENCES

1. Zhang H, Yee D, Wang C. Quantum dots for cancer diagnosis and therapy: biological and clinical perspectives. *Nanomedicine (Lond).* 2008;3:83–91.
2. Cai W, Shin DW, Chen K, et al. Peptide-labeled near-infrared quantum dots for imaging tumor vasculature in living subjects. *Nano Lett.* 2006;6:669–676.
3. Tada H, Higuchi H, Wanatabe TM, Ohuchi N. In vivo real-time tracking of single quantum dots conjugated with monoclonal anti-HER2 antibody in tumors of mice. *Cancer Res.* 2007;67:1138–1144.
4. Kim S, Lim YT, Soltesz EG, et al. Near-infrared fluorescent type II quantum dots for sentinel lymph node mapping. *Nat Biotechnol.* 2004;22:93–97.
5. Gao X, Cui Y, Levenson RM, Chung LW, Nie S. In vivo cancer targeting and imaging with semiconductor quantum dots. *Nat Biotechnol.* 2004;22:969–976.
6. Tang H, Yang K, Zhao C, Bai Y, Huang H. In situ visual imaging and in vivo distribution of head and neck squamous cell carcinoma in mice by near-infrared fluorescent quantum dots epidermal growth factor receptor monoclonal antibody probe. *Hua Xi Kou Qiang Yi Xue Za Zhi.* 2012;30:568–573.
7. Tang G. Process of muti-targeted molecular imaging. *Nucl Technol.* 2011;34:765–771.
8. Cai W, Chen K, Li ZB, Gambhir SS, Chen X. Dual-function probe for PET and near-infrared fluorescence imaging of tumor vasculature. *J Nucl Med.* 2007;48:1862–1870.
9. Cai W, Chen X. Anti-angiogenic cancer therapy based on integrin $\alpha_v\beta_3$ antagonism. *Anticancer Agents Med Chem.* 2006;6:407–428.
10. Xiong JP, Stehle T, Zhang R, et al. Crystal structure of the extracellular segment of integrin $\alpha_v\beta_3$ in complex with an Arg-Gly-Asp ligand. *Science.* 2002;296:151–155.
11. Glover SC, Tretiakova MS, Carroll RE, Benya RV. Increased frequency of gastrin-releasing peptide receptor gene mutations during colon-adenocarcinoma progression. *Mol Carcinog.* 2003;37:5–15.
12. Nanda PK, Pandey U, Bottenus BN, et al. Bombesin analogues for gastrin-releasing peptide receptor imaging. *Nucl Med Biol.* 2012;39:461–471.
13. Zhang X, Cai W, Cao F, et al. ^{18}F-labeled bombesin analogs for targeting GRP receptor-expressing prostate cancer. *J Nucl Med.* 2006;47:492–501.
14. Li ZB, Wu Z, Chen K, Ryu EK, Chen X. ^{18}F-labeled BBN-RGD heterodimer for prostate cancer imaging. *J Nucl Med.* 2008;49:453–461.
15. Yan Y, Chen K, Yang M, Sun X, Liu S, Chen X. A new ^{18}F-labeled BBN-RGD peptide heterodimer with a symmetric linker for prostate cancer imaging. *Amino Acids.* 2011;41:439–447.
16. Tang G, Wang H, Liang X, Huang T, Hu K. Radiosynthesis and preliminary evaluation of ^{18}F-FB-PEG-BBN-beta-Glu-RGD-QD as a new targeted dual-receptor dual-modality probe for tumor imaging [abstract]. *J Nucl Med.* 2012;53(suppl 1):1699.
17. Tang G, inventor; Yuehua Cheng, assignee. Symmetrical bifunctional coupling linker and its coupling molecular imaging agents. China patent no. 2011102754372. March 28, 2012.
18. Hu KZ, Wang H, Huang T, et al. Synthesis and biological evaluation of *N*-(2-[^{18}F]fluoropropionyl)-L-methionine for tumor imaging. *Nucl Med Biol.* 2013;40:926–932.
19. Hu KZ, Wang H, Tang G, et al. Automated synthesis of symmetric integrin $\alpha_v\beta_3$-targeted radiotracer [^{18}F]FP-PEG_3-β-Glu-RGD_2. *J Radioanal Nucl.* 2014;299:271–276.
20. Ebenstein Y, Nahum E, Banin U. Tapping mode atomic force microscopy for nanoparticle sizing: tip—sample interaction effects. *Nano Lett.* 2002;2:945–950.
21. Akerman ME, Chan WC, Laakkonen P, Bhatia SN, Ruoslahti E. Nanocrystal targeting in vivo. *Proc Natl Acad Sci USA.* 2002;99:12617–12621.
22. Yang RS, Chang LW, Wu JP, et al. Persistent tissue kinetics and redistribution of nanoparticles, quantum dot 705, in mice: ICP-MS quantitative assessment. *Environ Health Perspect.* 2007;115:1339–1343.
23. Chen ML, He YJ, Chen XW, Wang JH. Quantum dots conjugated with Fe_3O_4-filled carbon nanotubes for cancer-targeted imaging and magnetically guided drug delivery. *Langmuir.* 2012;28:16469–16476.
24. Liu Y, Ai K, Yuan Q, Lu L. Fluorescence-enhanced gadolinium-doped zinc oxide quantum dots for magnetic resonance and fluorescence imaging. *Biomaterials.* 2011;32:1185–1192.
25. Kluza E, Van Der Schaft DW, Hautvast PA, et al. Synergistic targeting of αvβ3 integrin and galectin-1 with heteromultivalent paramagnetic liposomes for combined MR imaging and treatment of angiogenesis. *Nano Lett.* 2010;10:52–58.
26. Robinson P, Neelon K, Schreier HJ, Roberts MF. β-glutamate as a substrate for glutamine synthetase. *Appl Environ Microbiol.* 2001;67:4458–4463.
27. Liu Z, Yan Y, Chin F, Wang F, Chen X. Dual integrin and gastrin-releasing peptide receptor targeted tumor imaging using ^{18}F-labeled PEGylated RGD-bombesin heterodimer ^{18}F-FB-PEG3-Glu-RGD-BBN. *J Med Chem.* 2009;52:425–432.
28. Hardman R. A toxicologic review of quantum dots: toxicity depends on physicochemical and environmental factors. *Environ Health Perspect.* 2006;114:165–172.